LANDMINE DETECTION BY MEANS OF GROUND PENETRATING RADAR: A RULE-BASED APPROACH

P.A. van Vuuren *

* *School of Electrical, Electronic and Computer Engineering, North-West University, Private Bag X6001, Potchefstroom, 2520, South-Africa. E-mail: pieter.vanvuuren@nwu.ac.za*

Abstract: For a humanitarian landmine detection system to be of practical value it has to meet the following criteria: detection must be performed in real-time from a moving platform; plastic mines must be reliably detected; and the false alarm rate should be kept to a minimum. Ground penetrating radar is a promising technology for the detection of landmines with low metal content. The improved algorithms presented in this paper can meet the above mentioned criteria to a large extent. Clutter removal is performed by an adaptive filter which removes virtually all background clutter in real time and can adapt to changing soil characteristics. Classification is performed by a new rule-based classifier capable of detecting both metal and plastic anti-tank mines. Despite the fact that the algorithms are currently implemented in Matlab®, mine detection can be performed on a vehicle moving at 9 km/h.

Key words: Landmine detection, ground penetrating radar, clutter removal

1. INTRODUCTION

Each year undetected landmines destroy many innocent lives. Although most nations agree that landmine removal is an important humanitarian problem, the reliable and efficient detection of buried landmines remains a challenging problem. Ground penetrating radar is a sensing technology that has delivered promising results in the detection of landmines with a low metallic content.

Traditionally, pattern recognition systems consist of three successive steps namely: preprocessing, feature extraction and final identification. Some researchers dispense with the first two steps and attempt to solve the pattern recognition problem in a single identification stage operating on the raw measured data. Inevitably, the lack of a concise set of features exposes the pattern recognizer (e.g. a neural network) with a sparsely populated, high-dimensional input space resulting in mediocre performance at best. Without a preprocessing step the data is often too noisy and/or dominated by unimportant phenomena to allow the extraction of usable features with high discriminatory abilities. Our practical experience tells us that a chain is only as strong as its weakest link. This advice also rings true in pattern recognition problems. Consequently *all* of the stages in a pattern recognition system have to be performed as optimally as possible.

In landmine detection via GPR the preprocessing step is primarily occupied with the removal of as much clutter as possible to facillitate successful landmine detection. To a large extent the GPR demining literature hasn't shown any significant new developments on the topic of clutter removal during the past few years. Although the clutter removal algorithms used at present are all quite good, they are far from perfect.

Section 2 of this paper presents an improved adaptive clutter removal algorithm which can be applied in real time. Clutter removal is typically followed by feature extraction and classification. In this paper, both of these steps are condensed into one. The classification approach presented in this paper is presented in section 3. The performance of both the clutter removal algorithm and the mine detection algorithm are separately evaluated in section 4, while final recommendations for future work are given in section 5.

This paper is the second paper in a two-part series on novel techniques that have been developed for the detection of landmines by means of ground penetrating radar (GPR). More details on the specific GPR array that has been used in this research can be found in the companion paper (Landmine detection by means of ground penetrating radar: a model-based approach). In the previous paper clutter removal was performed on the original frequency domain data delivered by the stepped-frequency continuous-wave GPR antenna array. The clutter removal procedure described in the previous paper however isn't amenable to an elegant real-time implementation. In the current paper the focus is on accurate landmine detection in real-time. A time-domain approach is followed throughout this paper.

2. CLUTTER REMOVAL

To be of practical worth, clutter removal procedures have to exhibit the following properties.

1. Real-time processing. In practice, mine clearance operations entail that large areas of land be processed. Time is therefore of the essence, which implies that landmine detection must be performed from a moving platform. It is therefore imperative that clutter removal be performed in real-time.

2. Adaptive behaviour. It is important that any clutter removal technique can adapt to changing soil conditions [1]. This calls for an adaptive model of the background clutter; one that can easily adapt to gradual variations in soil properties, but is too slow to track the abrupt changes caused by mine reflections.

3. Reduced correlation between A-scans of empty soil (i.e. without any mines), but improved correlation between A-scans containing mine responses.

As mentioned in the previous paper, the basic idea behind a number of existing clutter removal procedures is to construct an adaptive model of the background present in each A-scan and then to subtract this model from the observed data. This process then emphasizes all rapid variations from the background clutter. Fundamentally, this process amounts to adaptive high-pass filtering.

Probably one of the simplest, yet effective solutions to this problem is to model the background clutter in the current A-scan as the weighted average of the previous N A-scans produced by the same antenna-element (i.e. the previous N A-scans in the down-track direction). Mathematically, this can be expressed as follows:

$$\hat{\mathbf{x}}_{ij} = \sum_{k=i-N}^{i-1} \left(\alpha_k \mathbf{x}_{kj} \right), \tag{1}$$

where $\hat{\mathbf{x}}_{ij}$ is the estimated A-scan at position (i,j), α_k is the weight reflecting the contribution of the k^{th} previous A-scan and $\mathbf{x}_{kj}$ is the measured A-scan at position (k,j). All A-scans are represented by $N_z \times 1$ vectors, where N_z refers to the number of samples in the vertical (depth) direction.

In terms of vector notation, the above model can be written as follows:

$$\hat{\mathbf{x}}_{ij} = \mathbf{X}\boldsymbol{\Theta}, \tag{2}$$

where $\mathbf{X}$ is a $N_z \times N$ matrix of the previous A-scans and $\boldsymbol{\Theta}$ is the $N \times 1$ vector of coefficients α_k.

If the coefficients of this weighted average are re-calculated for every new cross-track B-scan, the model can adapt to changing conditions. The number of previous A-scans (N) determines the ability of the model to adapt to changing conditions: the larger N becomes, the more inertia the model shows against change. Optimal weights can be obtained by minimizing the difference between the background model and the current A-scan.

A least-squares solution for the coefficient vector can be found by means of the Moore-Penrose pseudo-inverse [2] as follows:

$$\boldsymbol{\Theta} = \mathbf{X}^{+}\mathbf{x}_{ij}, \tag{3}$$

where $\mathbf{X}^{+} = (\mathbf{X}^T\mathbf{X})^{-1}\mathbf{X}^T$.

Finally, the decluttered version of any A-scan $\left(\tilde{\mathbf{x}}_{ij}\right)$ can then be obtained by subtracting the model of the background clutter $\left(\hat{\mathbf{x}}_{ij}\right)$ in the A-scan from the A-scan $\left(\mathbf{x}_{ij}\right)$ as follows:

$$\tilde{\mathbf{x}}_{ij} = \mathbf{x}_{ij} - \hat{\mathbf{x}}_{ij} \tag{4}$$

The above mentioned clutter removal procedure is undeniably very simple. It is however very effective as the results presented in section 4.1 show. The next step in mine detection entails feature extraction and classification. In this paper both of these steps are combined in a single rule-based detection algorithm.

3. RULE-BASED MINE DETECTION

Two of the tell-tale signs of the presence of a mine in GPR data are the so-called hyperbolas and concentric circles. As figure 1 shows, these patterns can be visible even in raw GPR data (in the case of metal anti-tank mines). It is no small wonder that hyperbolas and circular patterns are used by human operators to detect mines.

Hyperbolas are in fact produced in GPR data by any distinct subsurface object due to the imperfect directivity of the radar antennae [3]. More specifically, radar signals are transmitted in relatively wide angle beams which allow the detection of objects some distance from the central axis of the beam. As a GPR antenna array moves along the surface, the accumulated reflections of these objects result in hyperbolic reflection patterns visible in vertical B-scans [4]. Concentric circles are visible in horizontal B-scans. These circular patterns are caused by the same mechanism as hyperbolas, but are limited to circular objects. (Buried pipes can be seen by hyperbolic patterns in vertical B-scans, but form linear patterns in horizontal B-scans.)

Other researchers have capitalized on the distinctive shapes of hyperbolic and circular reflections to design mine detection systems. One innovative approach was to perform clutter removal by means of a digital two-dimensional high-pass filter whose pass-band was determined by the frequency

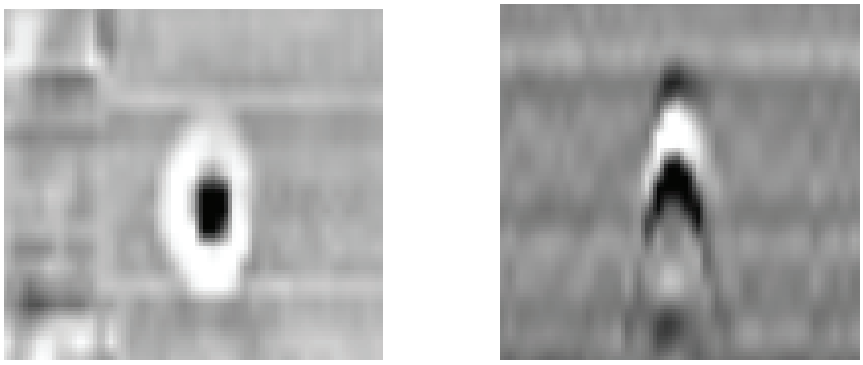

(a) Concentric circles in a horizontal B-scan (b) Hyperbolas in a vertical B-scan

Figure 1: Circles and hyperbolas present in raw GPR data

response of hyperbolic patterns [5]. Their approach did improve the signal to clutter ratio of the data without significantly reducing the quality of mine reflections. However, as mentioned previously, hyperbolic patterns aren't unique to mines - in fact, pebbles also frequently cause such patterns.

Similarly, the idea to use *only circular patterns* in GPR data as an indicator of the presence of mines isn't a new one. Some authors followed an image processing approach in which each horizontal B-scan is regarded as an image [6] and [7]. Features are then extracted from each image to measure the properties (such as the eccentricity and compactness) of any circular objects in the image. The resultant features are then used by either rule-based classifiers [6] or neural networks [7] to come to a final decision on the identity of the buried object. Classifiers based on features that measure some aspect of the circular patterns have obtained some success on practical GPR data [7]. Unfortunately the computational cost incurred by the required feature extraction process is quite high, since the circular nature of the patterns are inferred indirectly from e.g. eigenvalue ratios obtained from moment matrices extracted from the B-scan image.

An alternative approach is to use the (circular) Hough transform to directly detect circular patterns in horizontal B-scans [8]. A major drawback of the Hough transform however is that it isn't accurate for small circles. (Even though the GPR antenna array used in this paper has an effective scan width of 1.575 m, the resultant image only has 21 pixels in the cross-track direction, which corresponds to a very small image.). Furthermore, the Hough transform is a computationally intensive procedure which precludes any real-time applications.

It is clear that a mine detection approach based on circular patterns shows promise if the computational cost can be decreased without a commensurate loss in detection accuracy.

3.1 *Algorithm overview*

Observation of horizontal B-scans show that mine responses exhibit the following characteristics:

- Circles consisting of a mixture of light and dark patterns.
- The radius of the outer ring increases as the observation depth is increased. The intensity of the outer ring however also quickly diminishes.
- The size of the rings correspond to the reflective properties of the mine. Metal mines are more reflective and are therefore also more visible.
- Sequences of concentric circles sometimes become visible. These are due to resonant scattering of the radar waves induced by the top and bottom edges of the mine [9].

The success of a rule-based mine detection algorithm depends heavily on the quality of features that are extracted or images that are used within the rule antecedents. If the presence of circular patterns in a horizontal B-scan are to be used to detect the presence of mines, it is therefore important to enhance the image sufficiently that the eventual classification becomes a mere formality. The entire classification algorithm will now be reviewed. Details of some of the intermediate steps in this algorithm are discussed in sections 3.2 to 3.5.

1. Extract a segment from the GPR C-scan. In the present version of the algorithm a "segment" is defined as a rectangular cylinder whose two horizontal dimensions are equal to the number of antennas in the cross-track direction. The height (depth) of the cylinder is determined by the desired maximum depth of the GPR scan. For the GPR data at our disposal, the segment encompasses a $21 \times 21 \times 160$ three-dimensional

matrix of data. The motivation for the large size of this segment is twofold. First is the relative rare occurence of landmines within any particular C-scan. Second is the relatively large size of the circular patterns within a horizontal B-scan. (In practical data the concentric rings associated with a metal anti-tank (AT) mine have a radius of anything between three and eight pixels, where each "pixel" refers to the reflection amplitude detected by a specific antenna within the entire GPR antenna array. In physical terms, these circular patterns therefore have radii stretching between 22.5 cm and 60 cm, for a cross-track channel spacing of 7.5 cm [10].)

2. For each depth index within the extracted segment, the following steps are then performed.
   (a) Emphasize both the darker and lighter pixels in each horizontal B-scan image. What is interpreted by the human visual system as a circular ring often actually consists of semi-circular arcs of quite different grayscale values, as can be seen in figure 2. This figure shows the response of a low metal content anti-tank (AT) mine after clutter removal has been performed. The image is shown purposefully small so that the circular patterns are more clearly visible. To facillitate automatic detection of circular patterns both lighter and darker grayscale values in the image have to be emphasized above the general background. The result of this nonlinear amplitude filter is shown in figure 4. A detailed discussion on this filter can be found in section 3.2.
   (b) Convert the filtered grayscale image into a binary image consisting of background pixels (black) and pixels in the vicinity of a semi-circular arc (white). An example of the thresholding process is given in figure 5. More details on this step can be found in section 3.3.
   (c) Fit a circle to the pixels identified by the thresholding process. The fitted circle can then be regarded as a model for the observed circular pattern.
   (d) Determine the validity of the aforementioned model (namely the fitted circle). This can be accomplished by calculating the accuracy of the fitted model with respect to the observed data. For more detail on the procedure to fit a circle to the data, as well as to validate the fitted circle, consult section 3.4.
   (e) If the fitted circle passes the test, its parameters (namely its centre position and radius) are used in a rule-based classifier to determine whether a mine is actually present or not.
3. Increment the down-track dimension index by a preset interval (e.g. half of the width of the extracted segment) and repeat the entire procedure from step 1.

Figure 2: Circular patterns caused by a plastic anti-tank mine

In the following paragraphs some detail aspects of the algorithm outlined in section 3.1 are presented.

3.2 *Contrast enhancement*

In image processing the subjective quality of an image can be improved by means of contrast enhancement [11]. Various techniques exist to perform contrast enhancement ranging from heuristic piecewise linear mappings of pixel grayscale values to histogram equalization. The disadvantage of piecewise linear mappings is that the resultant mapping from input to output pixel intensities is non-smooth, which might result in unexpected edges being artificially introduced in the image. Histogram equalization on the other hand strives to obtain a more uniform distribution of grayscale values throughout the image. This powerful and elegant technique does however tend to amplify noise in the image.

A useful alternative to piecewise linear contrast enhancement is the logistic function. Also known as the sigmoid function in the neural network literature, the logistic function represents a smooth nonlinear mapping between an arbitrary input space and the unit interval. As can be seen in figure 3 the logistic function can be easily modified to accomplish any desired mapping between the input and output space. Mathematically, this function can be expressed as follows:

$$y = \frac{1}{1 + e^{-a(x-b)}}, \tag{5}$$

where x represents the original grayscale value of a pixel, y is the transformed grayscale value and a and b are two parameters that control the particular nature of the mapping. The crossover point of the logistic function (defined as the input value for which the function value is equal to 0.5.) is determined by b, while a controls the gradient of the function at its crossover point.

As is evident in figure 2 circular patterns often consist of a combination of light and dark pixels arranged in semi-circular arcs. The objective of

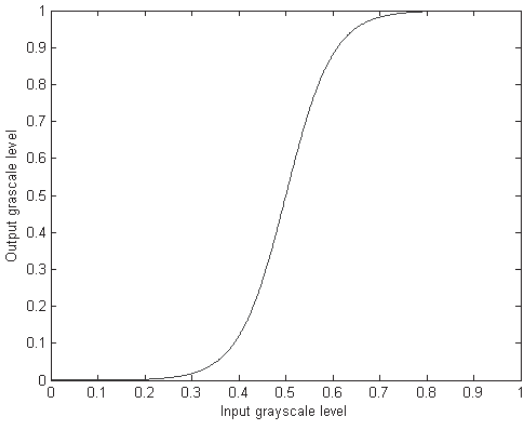

Figure 3: The logistic function

image improvement in this context therefore entails enhancing the contrast of both light and dark pixels in comparison with the general background. This can be accomplished by the sum of two separate logistic functions, one responsible for enhancing dark pixels (y_1) and another responsible for enhancing light pixels (y_2). The resultant amplitude filter is summarised in (6).

$$\begin{aligned} y &= y_1 + y_2 \\ &= \frac{1}{1+e^{b(x-a)}} + \frac{1}{1+e^{-c(x-d)}} \end{aligned} \tag{6}$$

It is clear from (6) that the performance of the resultant filter is determined by the values of its four parameters: a, b, c and d. Optimal values for these parameters were obtained through a process of trial and error. In this context, "optimal" parameters are defined as those parameter values that result in the isolation of only those pixels that form part of a circular arc. The final filter function (obtained through a process of visual evaluation of the results obtained by various sets of filter coefficients) is given by

$$y = \frac{1}{1+e^{50(x-0.5)}} + \frac{1}{1+e^{-50(x-0.6)}}. \tag{7}$$

Example results of the contrast enhancement process are given in figure 4. The input image for the nonlinear amplitude filter is a decluttered horizontal B-scan. Figure 4(a) shows a B-scan of a metal AT mine. The dark and light arcs that comprise the circular patterns are clearly visible in this image. After the nonlinear amplitude filter of (7) is applied to the image in figure 4(a) only a subset those pixels that form part of the circular pattern are isolated, as can be seen in figure 4(b). It is possible to include a larger subset of the pixels on the circular patterns by merely adjusting the parameters in (6). Such a larger subset does however come at the cost of more noise in the filtered image. Increased noise levels in turn leads to difficulty in fitting an accurate circle to the isolated pixels.

3.3 Thresholding

At this stage of the process the original B-scan image is reduced to a predominantly dark image containing a small set of lighter pixels that are located in the vicinity of a circular pattern (see figure 4(b)). The isolated pixels however still have differing grayscale values, as is also evident in figure 4(b). In order to be able to fit a circle to the observed circular pattern, it is necessary to distinguish unambiguously between the pixels that are definitely on the circular pattern and those who aren't. This choice can be made by converting the grayscale image to a black and white image by means of a thresholding function.

More specifically, if a pixel's grayscale value is less than 0.5 it is converted to zero (black). If however a pixel's grayscale value is 0.5 or greater, it is converted to one (white). An example of the result of the thresholding process is presented in figure 5.

The choice of the threshold grayscale value is determined by the distribution of grayscale values in the enhanced image. As an example, figure 6 shows a histogram of the grayscale values in the enhanced image in figure 4(b). Clearly, the vast majority of the pixels in the image are in fact part of the background, with only a very small number with grayscale values exceeding 0.5. If the threshold is chosen too low, spurious pixels are included in the dataset that is to be used for the circle fitting algorithm. If the threshold is chosen too high, some of the pixels which should have been on the circle are omitted. Either error will result in inaccurate circle fitting. Typically, the threshold should be chosen to be somewhere at the bottom of the valley in the histogram in figure 6. A threshold value of 0.6 was used to obtain the results in presented in this paper.

3.4 Circle fitting

Algorithms that fit circles to observed data point can be divided in two main categories, namely: geometric and algebraic algorithms [12]. Geometric algorithms minize the geometric distance between the model (fitted circle) and the data and are often implemented by means of orthogonal least squares. The *geometric distance* is in essence the difference between the radius of the fitted circle and the "true" radius of the circle which gave rise to the observed data. Algebraic algorithms on the other hand minimize the algebraic distance (which is the difference between the squared radius of the fitted circle and the squared radius of the true underlying circle) between the observed data and the fitted circle.

Geometric algorithms are often regarded as being

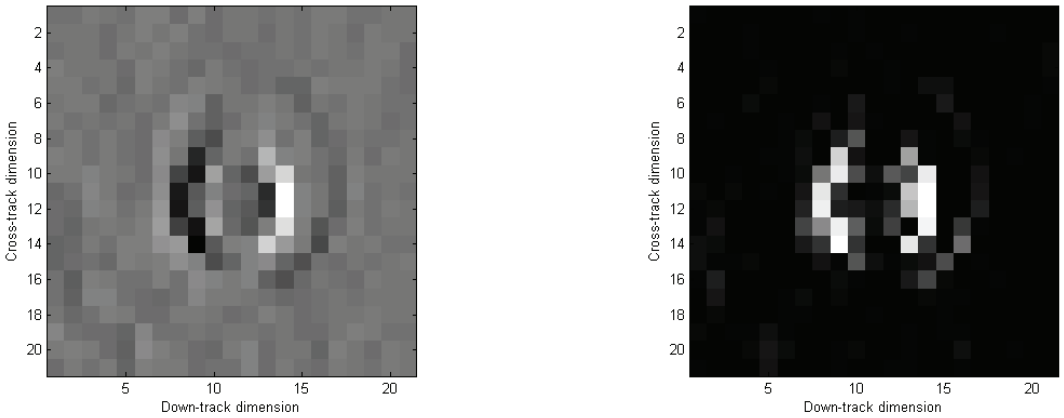

(a) Decluttered horizontal B-scan of a metal AT mine (b) Result of nonlinear amplitude filtering

Figure 4: Contrast enhancement by means on logistic filters

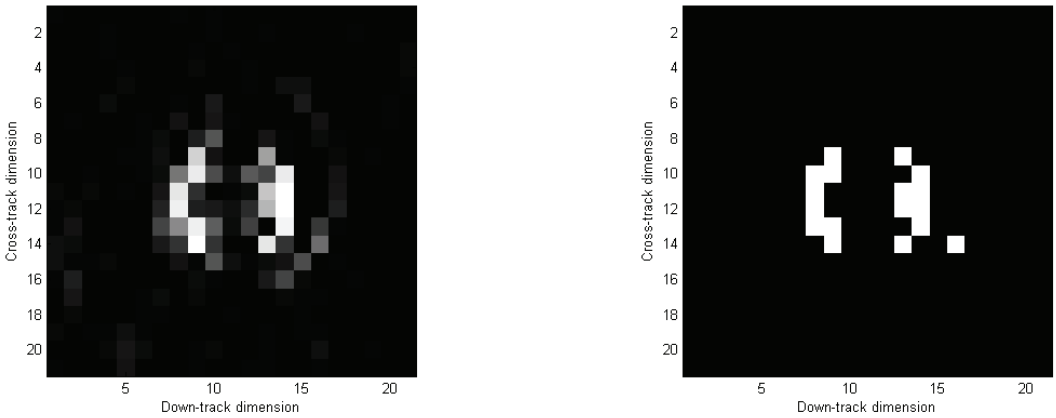

(a) Image after contrast enhancement (b) Binary image after thresholding

Figure 5: Isolation of circle pixels by means of thresholding

more accurate than algebraic algorithms, but are also iterative and therefore more computationally intensive. The relative inaccuracy of algebraic algorithms should however be seen in the context that the differences in the accuracy between algebraic and geometric algorithms can only be revealed by higher order error analysis [12]. The slight loss in accuracy incurred by an algebraic circle fitting algorithm is therefore handsomely compensated for by its speed.

Obtaining a least-squares fit for a circle is a nonlinear problem. In algebraic algorithms parameter substitutions are used to convert this nonlinear problem into a linear problem. Probably the fastest algebraic circle fitting algorithm is the Kåsa algorithm [13]. Compared to other algebraic algorithms it does have a bias towards small circles (i.e. the radius of the fitted circles are consistently slightly too small). This shortcoming is however irrelevant for the application in mind, as we'll see when the classification rule is discussed in section 3.5.

Figure 7 shows the circle fitted on the data obtained from the binary image in figure 5(b). The circle in figure 7 is superimposed on the enhanced image of figure 5(a) to show that the fitted circle is indeed an accurate model for the observed circular pattern.

The acceptance of any mathematical model is however subject to its validation. This principle also holds true in this landmine detection algorithm, since a lot depends on the accuracy of the fitted circle. The next step of the mine detection algorithm is therefore to ensure the quality of the fitted circle.

The quality of the fitted circle can be assessed by the following three self-evident rules:

(a) The centre of the fitted circle must be within the

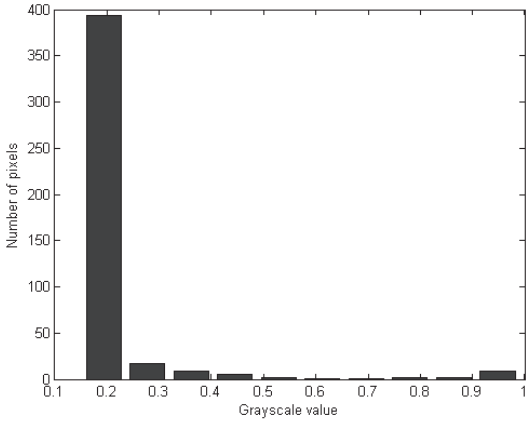

Figure 6: Histogram of grayscale values in the enhanced image

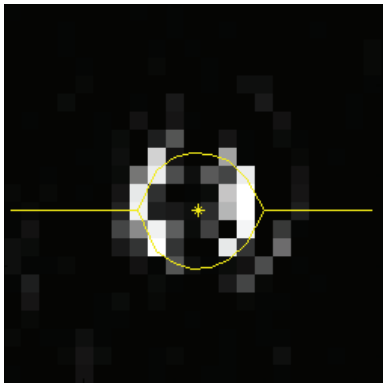

Figure 7: Circle fitted to a circular pattern

boundaries of the image.

(b) The diameter of the fitted circle must fit inside the boundaries of the image.

(c) And most importantly, the fitted circle must be a good description of the underlying pattern in the data.

The last consideration is in essence the accuracy of the fitted model and can be conveniently measured with the so-called coefficient of determination [14]. This measure is often used in system identification and can be interpreted as the "...fraction of the raw variation in y accounted for using the fitted equation." [14]. Mathematically, the coefficient of determination can be expressed as follows:

$$R^2 = \frac{\sum_i (y_i - \bar{y})^2 - \sum_i (y_i - \hat{y}_i)^2}{\sum_i (y_i - \bar{y})^2}, \qquad (8)$$

where y_i refers to the i^{th} measured datapoint (the row number of a pixel), $\bar{y}$ represents the average value of the measured datapoints and $\hat{y}_i$ signifies the value of the fitted circle corresponding to the i^{th} measured datapoint.

If the R^2-value of a fitted circle is less than a prescribed value, the model is rejected. In that case it can be concluded that there is no circular pattern present in the data, which in turn leads to the conclusion that no mine is present at least at the depth of the current B-scan. The threshold against which the R^2-value of the fitted circle is compared determines the stringency of the detection algorithm. Low values for this threshold result in numerous false alarms. If the threshold value for the fitted circle's quality is however too high, some mines might escape detection. In the present version of the algorithm only circles with an accuracy exceeding 95 percent were retained.

3.5 *Classification rule*

As mentioned in section 3.1, the reflections caused by landmines have a number of characteristic properties. In short, as the depth index increases a number of concentric rings fan out from a common centrepoint. This observation forms the basis of a rule with which landmine detection can be performed. It is important to note that the precise size of the fitted circles is not as important as the reliable detection and placement of the circles in the first place. Since the rings are arranged in concentric patterns and the Kåsa algorithm is biased towards smaller circles it invariably works out in practice that the radius of the fitted circle remains roughly constant as the depth increases.

The following rule can therefore be used to detect mines from a sequence of B-scans:

IF two or more circles occur in consecutive B-scans AND IF their centrepoints remain approximately constant AND IF their radii also remain approximately constant THEN a landmine occurs at the horizontal position and depth of the fitted circles.

From the above mentioned rule it is evident that one advantage of this approach to mine detection is that it is quite easy to pinpoint the position of the mine in three dimensions.

4. RESULTS

The algorithms discussed in sections two and three were implemented on the same dataset that was used in the companion paper. Similar measures are also used to assess the results as in the previous paper.

4.1 *Clutter removal results*

The clutter removal algorithm presented in this paper only has a single adjustable parameter, namely the number (N) of previous A-scans that are included in the weighted average. It was found experimentally

that the best balance between the quality of clutter removal and computational cost is struck for $N = 2$.

Figure 8 shows a horizontal B-scan taken at a specific depth both before and after clutter removal. Small differences between the different antenna-elements cause interference patterns in the raw data. The result are the linear patterns present in figure 8(a) (where they resemble car tracks). From figure 8(b) it is clear that all antenna-related noise has been removed by the clutter removal procedure of (4).

The quality of clutter removal algorithms can also be measured more objectively by the average level of cross-correlation present in the data after it has been processed. Figure 9 shows the average degree of peak cross-correlation for every 3×3 neighbourhood of A-scans in the data. Figure 9(a) shows the average degree of correlation of neighbouring A-scans after application of a time-domain principal component based clutter removal algorithm [15]. This figure should be interpreted as a top-down view of an area of ground which has been scanned with a ground-penetrating radar. Areas showing high degrees of correlation may be indicative of interesting subsurface objects or soil layers. Superimposed on this figure are the positions of known mines (indicated with black squares). Clearly, there is room for improvement in the clutter removal algorithm since large areas of ground are shown to have highly correlated A-scans.

The average degree of cross-correlation was also calculated for the new clutter removal algorithm (figure 9(b)). Clearly, the new clutter removal algorithm removes almost all of the background reflections from the data with the result that the A-scans are almost entirely decorrelated (with the exception of the immediate vicinity of the two metal AT mines).

Probably the most attractive feature of the improved clutter removal algorithm is its speed. The new algorithm requires 3.7 ms to process an entire cross-track B-scan, which makes real-time implementation possible. If the reader bears in mind that all of the results presented in this paper were obtained by means of Matlab®, one could easily expect another twofold improvement if the algorithm is implemented in C.

4.2 *Adaptability of the background model*

The new clutter removal algorithm can adapt to changing soil conditions. This property is due to the fact that the background clutter present in each A-scan is modelled by the weighted average of the previous A-scans in the down-track direction. One could however wonder whether the model's coefficients are in fact adapted in response to the changing soil conditions or whether the algorithm merely gravitates to a fixed filter after a few rows of A-scans.

In section 4.1 it is reported that only two prior A-scans are necessary to obtain a useful weighted average. The background clutter in any A-scan can therefore be modelled as in (9). The model in (9) is in effect a moving average low-pass filter whose filter coefficients are adaptively calculated. The bandwidth of a moving average low-pass filter is inversely related to the window width. A short window (as in the filter in (9)) therefore corresponds to a low-pass filter with a large bandwidth. Consequently, the decluttered A-scans therefore only contain very high frequencies.

$$\hat{\mathbf{x}}_{ij} = \theta_1 \mathbf{x}_{(i-1)j} + \theta_2 \mathbf{x}_{(i-2)j}. \tag{9}$$

The distributions of the coefficients θ_1 and θ_2 in (9) are given in the histograms presented in figure 10. These histograms were obtained from the filter coefficients calculated for each and every A-scan in the entire available C-scan of data. Clearly, the values for both coefficients are distributed continuously over quite small ranges. Furthermore, the coefficients seem to be normally distributed.

The distribution of the filter coefficients calculated for each A-scan are given as a function of the physical location of the corresponding A-scan in figure 11(a) and (b). Although it seems that the filter coefficients were chosen at random, a careful study of both figures reveals that small regions of similar coefficient values are present in the images. This observation supports the conclusion that the model in (9) does indeed adapt to changing local soil conditions.

4.3 *Landmine detection results*

Although the rule-based classifier seems quite simplistic compared to other classifiers, its performance is nothing to be scoffed at. As figure 12 shows, the rule-based classifier can correctly identify metal AT mines as well as a plastic AT mine. In this figure, the positions of known mines are indicated by cyan squares, while red stars indicate the positions where the algorithm thought there were mines.

Although this classifier can detect metal and non-metal AT mines, its false alarm rate is in need of attention, as can be clearly seen in figure 12. Furthermore, the rule-based algorithm couldn't detect plastic anti-personnel (AP) mines. An analysis of the GPR data at the positions of the false alarms show that there are indeed circular patterns present at the locations of the false alarms. As figure 12 shows, false alarms frequently occur near the known locations of meerkat tunnels as well as on the boundary between the sandpit and normal soil.

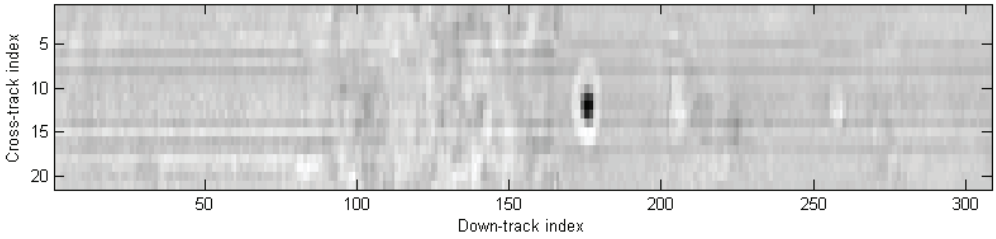

(a) Before clutter removal

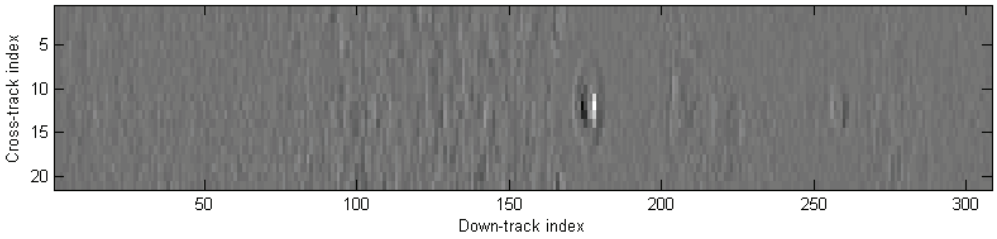

(b) After clutter removal

Figure 8: Subjective evaluation of the quality of clutter removal

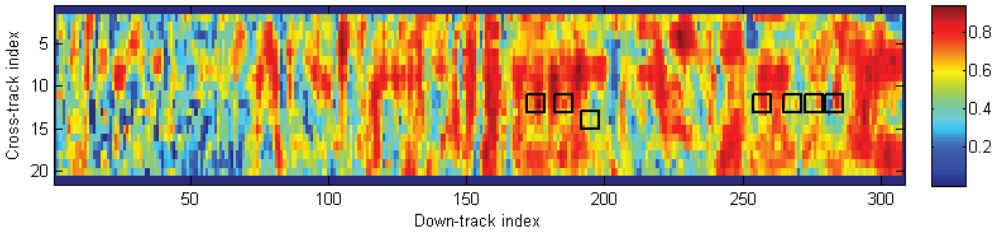

(a) Time domain principal component based filtering

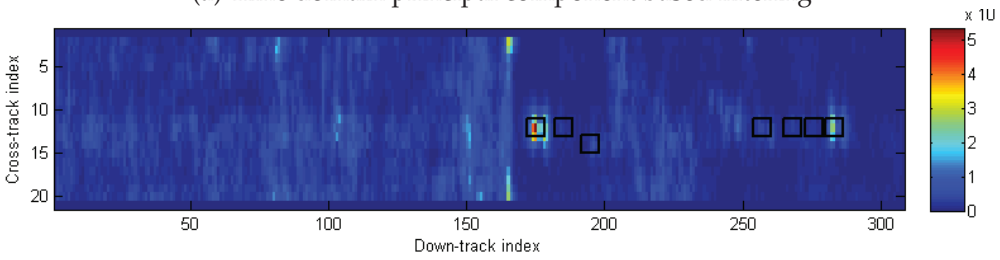

b) New clutter removal algorithm

Figure 9: Comparison of the cross-correlation present in the data after clutter removal

Indeed, there are a number of subsoil objects with GPR reflections quite similar to those of mines.

Another (more serious) problem is that the rule-based algorithm couldn't detect any AP mine. The available GPR data is partly to blame for this state of affairs. In this specific dataset the spacing between consecutive cross-track B-scans is 10 cm. If the small dimensions of e.g. an M-14 mine are taken into consideration, it is no small wonder that the presence such mines are well nigh invisible in the GPR data

One advantage of the rule-based classifier is its speed. On average it requires 417 μs to process an entire cross-track B-scan. If this is added to the 3.7 ms per cross-track B-scan required by the clutter removal algorithm, the entire duration is 4.1 ms. This is almost negligible compared to the 35.7 ms required to obtain the GPR cross-track B-scan data in the first place. If successive cross-track B-scans are separated by a distance of 10 cm (as is the case with the available data), the landmine detection (including radar measurement) can be performed at a maximum speed of 2.51 m/s or 9.04 km/h.

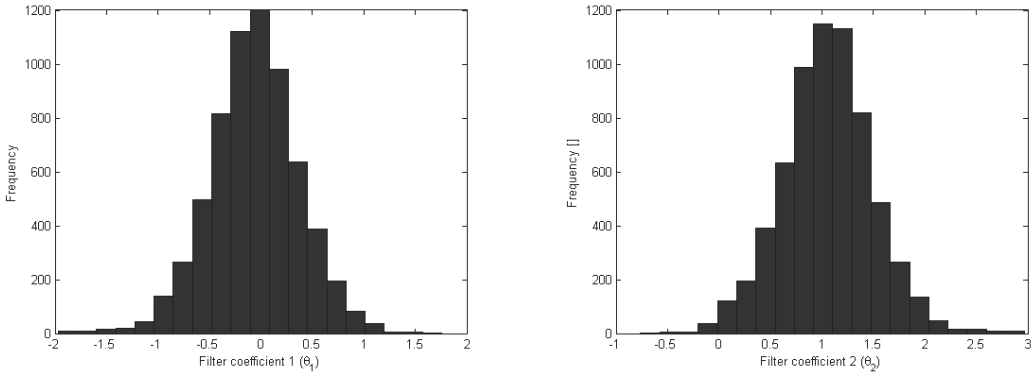

Figure 10: Histograms of the values of θ_1 and θ_2 in (9)

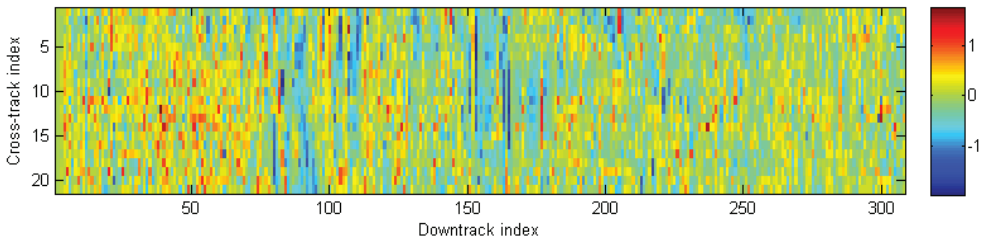

(a) Values of θ_1

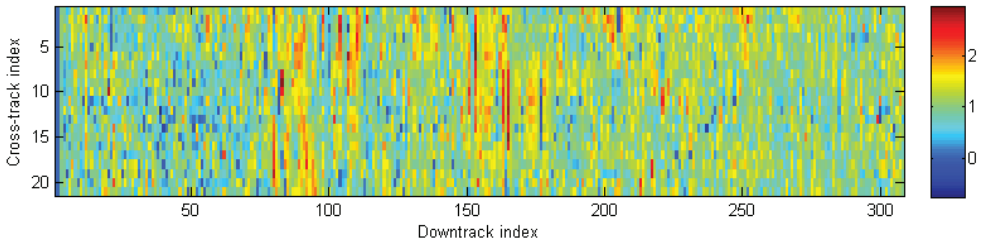

b) Values of θ_2

Figure 11: Filter coefficient values as a function of physical location

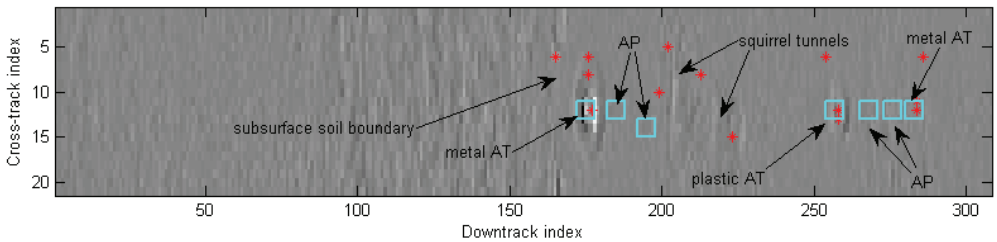

Figure 12: Detection results

5. CONCLUSION

Compared to the existing GPR literature, the performance of the rule-based classifier of section 3 is quite promising. In fact, one can state with a certain degree of confidence that real time GPR detection of plastic AT mines is feasible. The improved clutter removal procedure described in section 2 not only removes almost all of the background clutter, but also in a time frame that allows real-time implementation. However, the following two concerns remain:

1. The false alarm ratio which is still too high. Improving the circle fitting algorithm will probably address this issue satisfactorily.

2. The inability of the classifier to detect plastic AP mines. This deficiency is however to be expected, since the particular mines are practically invisible even in the decluttered data. The resolution of the original raw GPR data can be improved by sampling the ground at finer intervals in the down-track direction. However, in certain soil conditions the difference in the permittivity of an AP mine and the surrounding soil will still be insufficient to make the mine visible in GPR data.

REFERENCES

[1] A. Van der Merwe and I. Gupta, "A novel signal processing technique for clutter reduction in GPR measurements of small, shallow land mines," *IEEE transactions on geoscience and remote sensing*, vol. 38, no. 6, pp. 2627–2637, November 2000.

[2] A. Ben-Israel and T. Greville, *Generalized inverses: theory and applications*. New-York: John Wiley & Sons, 1974.

[3] S. Perrin, E. Duflos, P. Vanheeghe, and A. Bibaut, "Multisensor fusion in the frame of evidence theory for landmines detection," *IEEE TRANSACTIONS ON SYSTEMS, MAN, AND CYBERNETICSPART C: APPLICATIONS AND REVIEWS*, vol. 34, no. 4, pp. 485–498, November 2004.

[4] O. Lopera, E. C. Slob, N. Milisavljevic, and S. Lambot, "Filtering soil surface and antenna effects from GPR data to enhance landmine detection," *IEEE Transactions on Geoscience and Remote Sensing*, vol. 45, no. 3, pp. 707 – 717, March 2007. [Online]. Available: http://dx.doi.org/10.1109/TGRS.2006.888136

[5] D. Potin, E. Duflos, and P. Vanheeghe, "Landmines ground-penetrating radar signal enhancement by digital filtering," *IEEE Transactions on Geoscience and Remote Sensing*, vol. 44, no. 9, pp. 2393 – 2406, 2006. [Online]. Available: http://dx.doi.org/10.1109/TGRS.2006.875356

[6] P. Gader, W.-H. Lee, and J. N. Wilson, "Detecting landmines with ground-penetrating radar using feature-based rules, order statistics, and adaptive whitening," *IEEE Transactions on Geoscience and Remote Sensing*, vol. 42, no. 11, pp. 2522 – 2534, 2004. [Online]. Available: http://dx.doi.org/10.1109/TGRS.2004.837333

[7] J. N. Wilson, P. Gader, W.-H. Lee, H. Frigui, and K. Ho, "A large-scale systematic evaluation of algorithms using ground-penetrating radar for landmine detection and discrimination," *IEEE Transactions on Geoscience and Remote Sensing*, vol. 45, no. 8, pp. 2560 – 2572, August 2007. [Online]. Available: http://dx.doi.org/10.1109/TGRS.2007.900993

[8] D. Daniels, *Ground penetrating radar*, 2nd ed. London: The Institution of Engineering and Technology, 2004.

[9] Daniels, "Ground penetrating radar fundamentals," Appendix to a report to the U.S. EPA region V, Tech. Rep., 2000.

[10] "V-series multi-channel antenna arrays for GPR: Mkt-ds-v-series-040810v1," 2010.

[11] R. Gonzalez and R. Woods, *Digital image processing*. Reading, Massachusetts: Addison-Wesley, 1992.

[12] A. Al-Sharadqah and N. Chernov, "Error analysis for circle fitting algorithms," *Electronic Journal of Statistics*, vol. 3, pp. 886–911, 2009.

[13] I. Kåsa, "A curve fitting procedure and its error analysis," *IEEE transactions on instrumentation and measurement*, vol. 25, pp. 8–14, 1976.

[14] S. Vardeman, *Statistics for engineering problem solving*. Boston: PWS, 1994.

[15] S. Tjora and E. Eide, "Evaluation of methods for ground bounce removal in GPR utility mapping," in *Tenth International Conference on Ground Penetrating Radar*, 2004.

NOTES

SAIEE AFRICA RESEARCH JOURNAL – NOTES FOR AUTHORS

This journal publishes research, survey and expository contributions in the field of electrical, electronics, computer, information and communications engineering. Articles may be of a theoretical or applied nature, must be novel and must not have been published elsewhere.

Nature of Articles

Two types of articles may be submitted:

- Papers: Presentation of significant research and development and/or novel applications in electrical, electronic, computer, information or communications engineering.
- Research and Development Notes: Brief technical contributions, technical comments on published papers or on electrical engineering topics.

All contributions are reviewed with the aid of appropriate reviewers. A slightly simplified review procedure is used in the case of Research and Development Notes, to minimize publication delays. No maximum length for a paper is prescribed. However, authors should keep in mind that a significant factor in the review of the manuscript will be its length relative to its content and clarity of writing. Membership of the SAIEE is not required.

Process for initial submission of manuscript

Preferred submission is by e-mail in electronic MS Word and PDF formats. PDF format files should be 'press optimised' and include all embedded fonts, diagrams etc. All diagrams to be in black and white (not colour). For printed submissions contact the Managing Editor. Submissions should be made to:

The Managing Editor, SAIEE Africa Research Journal,
PO Box 751253, Gardenview 2047, South Africa.
E-mail: researchjournal@saiee.org.za

These submissions will be used in the review process. Receipt will be acknowledged by the Editor-in-Chief and subsequently by the assigned Specialist Editor, who will further handle the paper and all correspondence pertaining to it. Once accepted for publication, you will be notified of acceptance and of any alterations necessary. You will then be requested to prepare and submit the final script. The initial paper should be structured as follows:

- TITLE in capitals, not underlined.
- Author name(s): First name(s) or initials, surname (without academic title or preposition 'by')
- Abstract, in single spacing, not exceeding 20 lines.
- List of references (references to published literature should be cited in the text using Arabic numerals in square brackets and arranged in numerical order in the List of References).
- Author(s) affiliation and postal address(es), and email address(es).
- Footnotes, if unavoidable, should be typed in single spacing.
- Authors must refer to the website: http: //www.saiee.org.za/arj where detailed guidelines, including templates, are provided.

Format of the final manuscript

The final manuscript will be produced in a 'direct to plate' process. The assigned Specialist Editor will provide you with instructions for preparation of the final manuscript and required format, to be submitted directly to:
The Managing Editor, SAIEE Africa Research Journal, PO Box 751253, Gardenview 2047, South Africa.
E-mail: researchjournal@saiee.org.za

Page charges

A page charge of R200 per page will be charged to offset some of the expenses incurred in publishing the work. Detailed instructions will be sent to you once your manuscript has been accepted for publication.

Additional copies

An additional copy of the issue in which articles appear, will be provided free of charge to authors.
If the page charge is honoured the authors will also receive 10 free reprints without covers.

Copyright